



**Fermi National Accelerator Laboratory**

FERMILAB-Conf-83/50-EXP  
7120.577

HADRON-HADRON ELASTIC SCATTERING AT LARGE MOMENTUM TRANSFERS\*

Roy Rubinstein

May 1983

\*Invited talk given at the Baltimore Meeting of the American Physical Society, April 18, 1983



Operated by Universities Research Association Inc. under contract with the United States Department of Energy

HADRON-HADRON ELASTIC SCATTERING AT LARGE MOMENTUM TRANSFERS

Roy Rubinstein

Fermi National Accelerator Laboratory, Batavia, Illinois 60510

ABSTRACT

Cross sections for  $\pi^\pm p$ ,  $K^\pm p$  and  $p^\pm p$  elastic scattering for incident momenta above a few tens of GeV/c and momentum transfers in the range  $1 \leq -t \leq 10 \text{ (GeV/c)}^2$  have recently been measured. The data are reviewed, and compared with existing models of elastic scattering.

## 1. INTRODUCTION

In the past three years, much new data has become available on hadron-hadron elastic scattering at incident momenta above a few tens of GeV/c and momentum transfers in the range  $1 \leq -t \leq 10^{(1)}$ . The data are primarily from two experiments, WA7 at CERN<sup>(2,3,4)</sup> (20 and 50 GeV/c) and E577 at Fermilab<sup>(5,6,7)</sup> (100 and 200 GeV/c).

Experimental techniques used by different groups to measure large  $-t$  elastic scattering have many common features, mainly determined by the difficulties of measuring cross sections  $d\sigma/dt$  as small as  $\sim 10^{-36} \text{ cm}^2 / (\text{GeV}/c)^2$ . For illustration, we show in Figure 1 the layout of E577. Spectrometers are used to record both of the outgoing particles, and there are cerenkov counters for particle identification in order to measure cross sections for more than one incident particle type simultaneously. Beam intensities typically are greater than  $10^7$  incident particles per second in order to have reasonable statistics out to large  $-t$ .

This report will discuss only a selection of the physics topics studied by the two experiments; the reader is referred to the published papers for other physics not covered here, and for more detailed descriptions of the experiments.

## 2. MODELS FOR HIGH MOMENTUM LARGE -t ELASTIC SCATTERING

In this report, I will compare data with three of the many models which have been proposed.

### (i) Geometrical Scaling<sup>(8)</sup>

The elastic scattering amplitude as a function of energy  $s$  and impact parameter  $b$ ,  $T(s,b)$ , is given by  $T(b/R(s))$ ; all of the energy dependence in the cross section is contained in the radial scale parameter  $R(s)$ . This leads to the following expressions for the total and elastic differential cross sections:

$$\sigma_T \sim R^2$$

$$d\sigma/dt \sim R^4 f(R^2 t)$$

where  $f$  is some universal function. Using the above two expressions, it is readily seen that a graph of  $d\sigma/dt$  normalized to the optical point, plotted against  $t\sigma_T$ , should be a universal curve.

### (ii) Chou-Yang Model<sup>(9)</sup>

In this diffraction (or geometrical) model, the amplitude for the elastic scattering of particle A on particle B is related to a transform of the product of the form factors of A and B; the assumption is made that the electromagnetic form factors for A

and B are the appropriate ones to use. This hypothesis can be tested in the pp case since considerable data on elastic scattering is available, and the electromagnetic form factors have been measured using electron-proton scattering. The agreement obtained between prediction and data is good, including prediction of the observed  $-t \sim 1.4$  dip (see, for example, reference 10).

(iii) QCD<sup>(11)</sup>

Lowest order QCD diagrams lead to the following expression for pp elastic scattering, expected to be valid at large s and t:

$$d\sigma/dt \sim s^{-10} (t/s)^{-8} ;$$

this gives

$$d\sigma/dt \sim s^{-10} \text{ at fixed } t/s \text{ (or fixed } \theta_{\text{cm}})$$

$$\text{and } d\sigma/dt \sim t^{-8} \text{ at fixed } s.$$

For  $\pi p$  scattering, the corresponding prediction is

$$d\sigma/dt \sim s^{-8} (t/s)^{-7}$$

### 3. PREVIOUSLY AVAILABLE DATA ABOVE $\approx 50$ GeV/c

Until  $\approx 1980$ , data existed for pp elastic scattering up to  $-t \approx 14$ ; np results extended to  $-t \approx 4$ , while  $\pi^{\pm}p$ ,  $K^{\pm}p$  and  $\bar{p}p$  data were available only up to  $-t \approx 2$ .

Some pp data<sup>(12-16)</sup> up to  $-t \approx 6$  is shown in Figure 2. The main feature is the emergence of a diffraction-like dip at  $-t \approx 1.4$ , together with a second maximum, for incident momenta above  $\approx 150$  GeV/c. Extensive data on the development of this dip structure as a function of incident momentum now exist. Results for np scattering show similar effects<sup>(17)</sup>.

Figure 3 gives pp results<sup>(15,16,18)</sup> at large  $-t$ , plotted in a form to illustrate the QCD-like behavior of the data; a fit is shown of the form  $|t|^{-n}$  with  $n = 8.6$ , close to the expected QCD value of  $n = 8$ .

### 4. ANTIPROTON-PROTON SCATTERING

The first important new result from the recent experiments is shown in Figure 4. The WA7 group<sup>(2)</sup> extended the 50 GeV/c  $\bar{p}p$  data to  $-t \approx 5$ , and discovered a dip at  $-t \approx 1.4$  followed by a second maximum; this effect was confirmed<sup>(6)</sup> at 100 GeV/c by E577. The shape of the  $t$  distribution is almost identical to that observed for pp scattering at ISR energies. Already, several explanations for the structure, together with predictions for its behavior with incident momentum, have been given. (See, for example, references 19 and 20).

## 5. PION-PROTON SCATTERING

The second major new result came when 200 GeV/c  $\pi^-p$  data became available from E577. Preliminary results were given in reference 5, and Figure 6 shows the current status of the data. As seen in the figure, the observed  $t$  distribution is smooth near  $-t \approx 1.4$ , unlike the baryon-proton case, but now a significant diffraction dip appears at  $-t \approx 4$ , followed by a second maximum and then a slow fall with increasing  $-t$ . This behavior was generally unexpected, although there had been at least one previous paper predicting such an effect<sup>(21)</sup>. Subsequent 50 GeV/c  $\pi^-p$  data<sup>(3)</sup> does not have this dip (see Figure 7), showing that there is a threshold energy for this behavior as in the  $pp$  case; however, 50 GeV/c  $\pi^+p$  data<sup>(3)</sup> does show a dip at about the same  $t$  value (Figure 8).

The pion form factor has been derived from the 200 GeV/c  $\pi^-p$  data using the Chou-Yang model<sup>(22)</sup>; Figure 9 shows the form factor obtained. The form factor agrees well with the pion electromagnetic form factor (not shown) obtained from pion electroproduction<sup>(23)</sup> where this information is available ( $-t < 2$ ), and the form factor slope near  $t = 0$  gives a value of the pion radius  $r_\pi = 0.66f$ , in good agreement with that obtained from  $\pi e$  scattering<sup>(24)</sup>.

The form factor agrees with the vector meson dominance model prediction for  $-t \leq 1$ , but there is significant disagreement at larger  $-t$ ; however, there is reasonable agreement with a QCD prediction<sup>(11)</sup> which is expected to be valid in the large  $-t$

region.

A comparison of the recent data with the QCD model prediction discussed in Section 2 (iii) is shown in Figure 9; since the prediction is expected to be valid only at large  $-t$ , we have restricted the data used in the comparison to the region above the  $-t \approx 4$  diffraction dip, specifically to  $-t \geq 4.9$ . The data is seen to be consistent with the expected  $|t|^{-7}$  dependence, although it would be more convincing if there were data at the same  $t/s$  but at two different incident momenta (as exists for the pp case shown in Figure 3). For this, 200 GeV/c measurements out to  $-t \approx 20$ , or 100 GeV/c measurements to  $-t \approx 10$  would be needed.

Although the data of Figure 9 is suggestive of agreement with the QCD prediction, it should be noted that neither set of experimental data is sufficiently accurate to verify the  $|t|^{-7}$  dependence itself, as illustrated in Figure 10; a comparison is given there with the corresponding pp case.

## 6. KAON-PROTON SCATTERING

50 GeV/c  $K^+p$  data<sup>(4)</sup> from WA7 (Figure 11) gives an indication of a dip at  $-t$  of 4, and a change of slope beyond that  $-t$  value. This behavior is similar to that in  $\pi^+p$  at the same momentum<sup>(3)</sup> (Figure 7).

The higher statistical accuracy of the WA7 and E577 data allows more detailed tests of the geometrical scaling model than previously possible; one such test is illustrated in Figure 12. In Figure 12a we show a comparison between 100 GeV/c  $\pi^-p$  and  $K^-p$

data<sup>(7)</sup> from E577, together with some earlier lower  $-t$  data (25) and the optical point<sup>(26-28)</sup>; it can be seen that the  $\pi^-p$  and  $K^-p$  distributions have different shapes; geometrical scaling predicts that when  $d\sigma/dt$  normalized to the optical point is plotted against  $t\sigma_T$  for the two reactions, the curves should become identical. This comparison is given in Figure 12b, and shows that there is a substantial violation of the geometrical scaling prediction.

#### 7. COMPARISON OF MESON-PROTON AND BARYON-PROTON SCATTERING

Although we have not illustrated it in this report, the E577 data shows that, over the  $t$  ranges measured, there is little difference between  $pp$  and  $\bar{p}p$  scattering, and little dependence of both on incident momentum. Similarly there is little difference between any of the meson-proton distributions, and little momentum dependence. (The differences of Figure 12 are relatively small). Meson-proton scattering, however, is substantially different from baryon-proton scattering, as seen in Figure 13 for 200 GeV/c  $\pi^-p$  and  $pp$ . Nevertheless, they do have common features - after a fall of many decades from the optical point, both show a diffraction dip (at  $-t \simeq 1.4$  for  $pp$  and  $-t \simeq 4$  for  $\pi^-p$ ) followed by a second maximum and then a relatively slow fall with increasing  $-t$ .

## 8. CONCLUSIONS

1. Hadron-hadron elastic scattering above  $\sqrt{s} \approx 50$  GeV/c is diffractive in the small  $-t$  region. There is little variation of any of the cross sections with incident momentum, and all (?) processes show a diffraction-like dip:

for  $pp$ ,  $\bar{p}p$  and  $np$ , this dip is at  $-t \approx 1.4$

for  $\pi^-p$ ,  $\pi^+p$  and possibly  $K^+p$ , the dip is at  $-t \approx 4$ .

2. At large  $-t$ ,  $pp$  elastic scattering data agree with the predictions of lowest order QCD, while  $\pi p$  is probably in agreement (although more data for  $\pi p$  is definitely needed).
3. Future data needed:
  - a)  $\pi p$  data to  $-t \approx 20$  at 100 and 200 GeV/c will help in testing the QCD prediction discussed above.
  - b)  $\bar{p}p$  scattering data out to  $-t \approx 2$  or greater at the CERN and Fermilab Colliders will enable tests of the diffractive nature of the small  $-t$  scattering to be carried out.

ACKNOWLEDGEMENTS

I wish to thank my colleagues of reference 5 for many valuable discussions on elastic scattering. This work was supported by the U.S. Department of Energy.

REFERENCES

1. In this report, the units for  $t$  are  $(\text{GeV}/c)^2$ .
2. Z. Asa'd, C. Baglin, S. Benso, R. Böck, K. Brobakken, L. Bugge, T. Buran, A. Buzzo, P. J. Carlson, M. Coupland, D. G. Davis, B. G. Duff, S. Ferroni, I. Gjerpe, V. Gracco, J. D. Hansen, P. Helgaker, F. F. Heymann, D. C. Imrie, T. Jacobsen, K. E. Johansson, K. Kirsebom, R. Lowndes, A. Lundby, G.J. Lush, M. Macri, R. Møllerud, J. Myrheim, M. H. Phillips, M. Poulet, L. Rossi, A. Santroni, G. Skjevling, S. O. Sørensen and M. Yvert, *Phys. Lett.* 108B, 51 (1982).
3. Z. Asa'd et al., *Phys. Lett.* 118 B, 442 (1982).
4. Z. Asa'd et al., CERN-EP/82-205 (to be published).
5. W. F. Baker, D. P. Eartly, J. S. Klinger, A. J. Lennox, R. Rubinstein, R. M. Kalbach, K. W. Krueger, A. E. Pifer, S. F. McHugh, D. H. Kaplan, P. Karchin and J. Orear, *Phys. Rev. Lett.* 47, 1683 (1981).
6. D. H. Kaplan et al., *Phys. Rev.* D 26, 723 (1982).
7. R. M. Kalbach et al., FERMILAB-Pub-83/20-EXP (to be published).
8. V. Barger et al., *Nucl. Phys.* B88, 237 (1975).
9. T. T. Chou and C. N. Yang, *Phys. Rev.* 170, 1591 (1968).
10. M. Kac, *Nucl. Phys.* B62, 402 (1973).

11. P. Lepage and S. Brodsky, Phys. Rev. D22, 2157 (1980).
12. C. Ankenbrandt et al., Phys. Rev. 170, 1223 (1968).
13. J. V. Allaby et al., Nucl. Phys. B52, 316 (1973).
14. G. Fidecaro et al., Phys. Lett. 105B, 309 (1981).
15. W. Faissler et al., Phys. Rev. D23, 33 (1981).
16. E. Nagy et al., Nucl. Phys. B150, 221 (1979).
17. C. DeHaven et al., Nucl. Phys. B148, 1 (1979).
18. G. Cocconi et al., Phys. Rev. 138, B165 (1965).
19. T. T. Chou and C. N. Yang, Phys. Rev. Lett. 46, 764 (1981).
20. M. M. Islam and J. P. Guillard, University of Connecticut preprint (1981).
21. S. C. Chan et al., Phys. Rev. D17, 802 (1978).
22. P. Karchin and J. Orear, Cornell University preprint CLNS-82/543 (1982).
23. C. J. Bebek et al., Phys. Rev. D13, 25 (1976) and D17, 1693 (1978).
24. E. B. Dally et al., Phys. Rev. Lett. 48, 375 (1982).
25. C. Akerlof et al., Phys. Rev. D14, 2864 (1976).
26. A. S. Carroll et al., Phys. Lett. 61B, 303 (1976) and 80B, 423 (1979).
27. L. A. Fajardo et al., Phys. Rev. D24, 46 (1981).
28. J. P. Burq et al., Phys. Lett. 77B, 438 (1978) and 109B, 111 (1982).

FIGURE CAPTIONS

Figure 1. Layout of Fermilab experiment E577.  $H_1-H_4$  are scintillation counter hodoscopes;  $P_1-P_8$  are proportional wire chamber arrays. Not shown are veto counters around the hydrogen target, helium bags in the forward spectrometer, monitor telescopes, and apparatus in the incident beam such as scintillation counters, proportional wire chambers, SWIC's, and a differential Cerenkov counter.

Figure 2. Some pp elastic scattering data, from references 12-16.

Figure 3. Elastic scattering cross section for pp multiplied by  $s^{10}$  plotted against  $-t/s$ ; data from references 15,16,18. Also shown is the line  $|t|^{-8.6}$ .

Figure 4. Data on  $\bar{p}p$  elastic scattering from references 2 and 6.

Figure 5. 200 GeV/c  $\pi^-p$  elastic scattering (reference 5).

Figure 6. 50 GeV/c and 200 GeV/c  $\pi^-p$  elastic scattering (references 3 and 5).

Figure 7.  $\pi^+p$  elastic scattering at 50 GeV/c (reference 3).

Figure 8. Pion form factor derived (ref. 22) from the 200 GeV/c  $\pi^-p$  data of reference 5, compared to a vector meson dominance curve and a QCD prediction (reference 11).

Figure 9. 50 GeV/c and 200 GeV/c  $\pi^-p$  data for  $-t > 4.9$ , from references 3 and 5, compared to the QCD prediction of  $|t|^{-7}$ .

Figure 10. Data on  $\pi p$  and  $pp$  elastic scattering (references 3,5,15); the curves show expected QCD dependences.

Figure 11.  $K^+p$  data at 50 GeV/c (reference 4).

Figure 12. Test of geometrical scaling, using data from references 7, 25-28.

Figure 13. Comparison of  $\pi^-p$  and  $pp$  elastic scattering at 200 GeV/c (references 5, 14, 15).

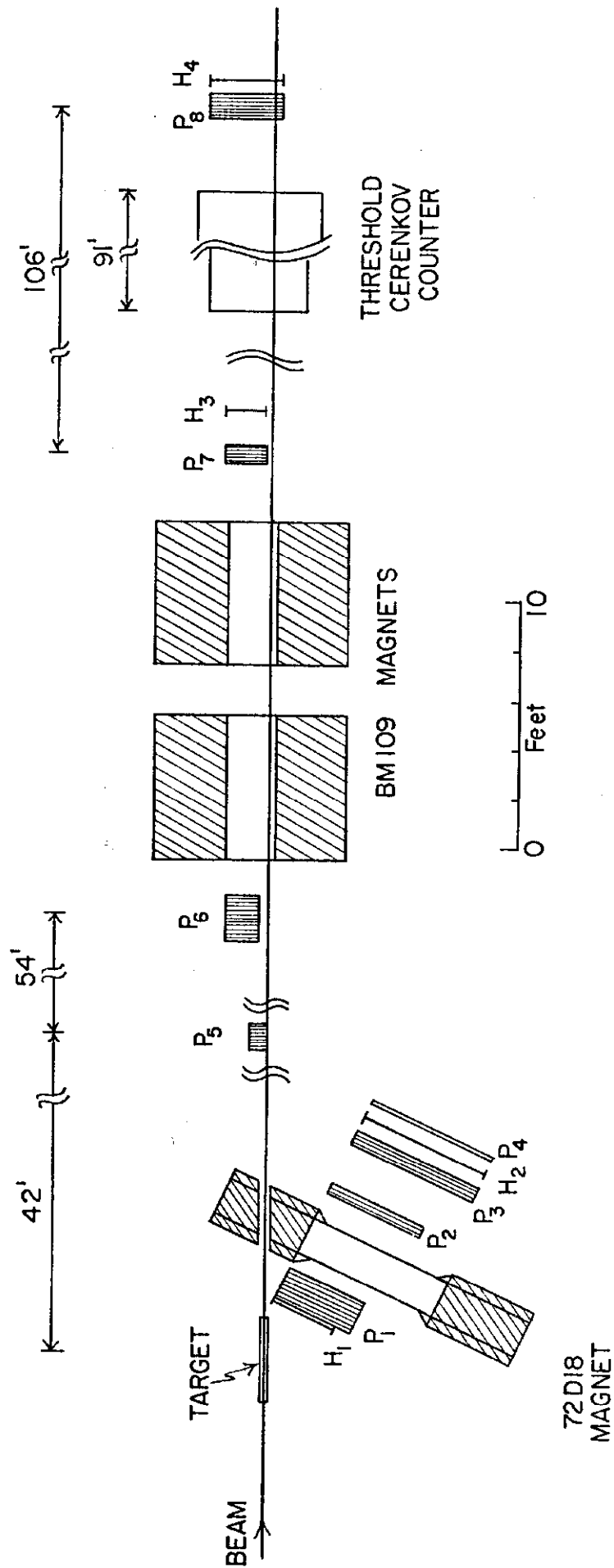


Figure 1

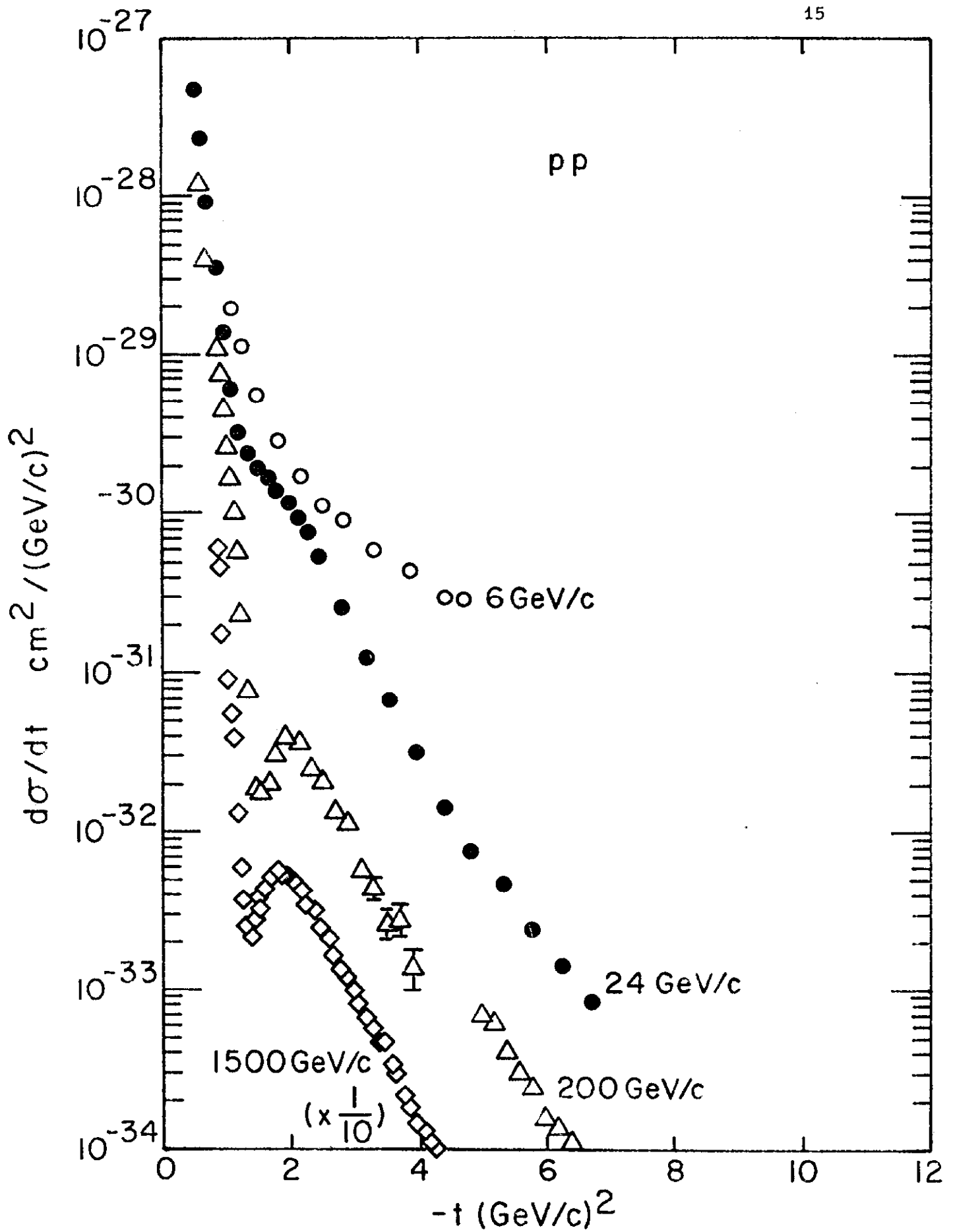


Figure 2

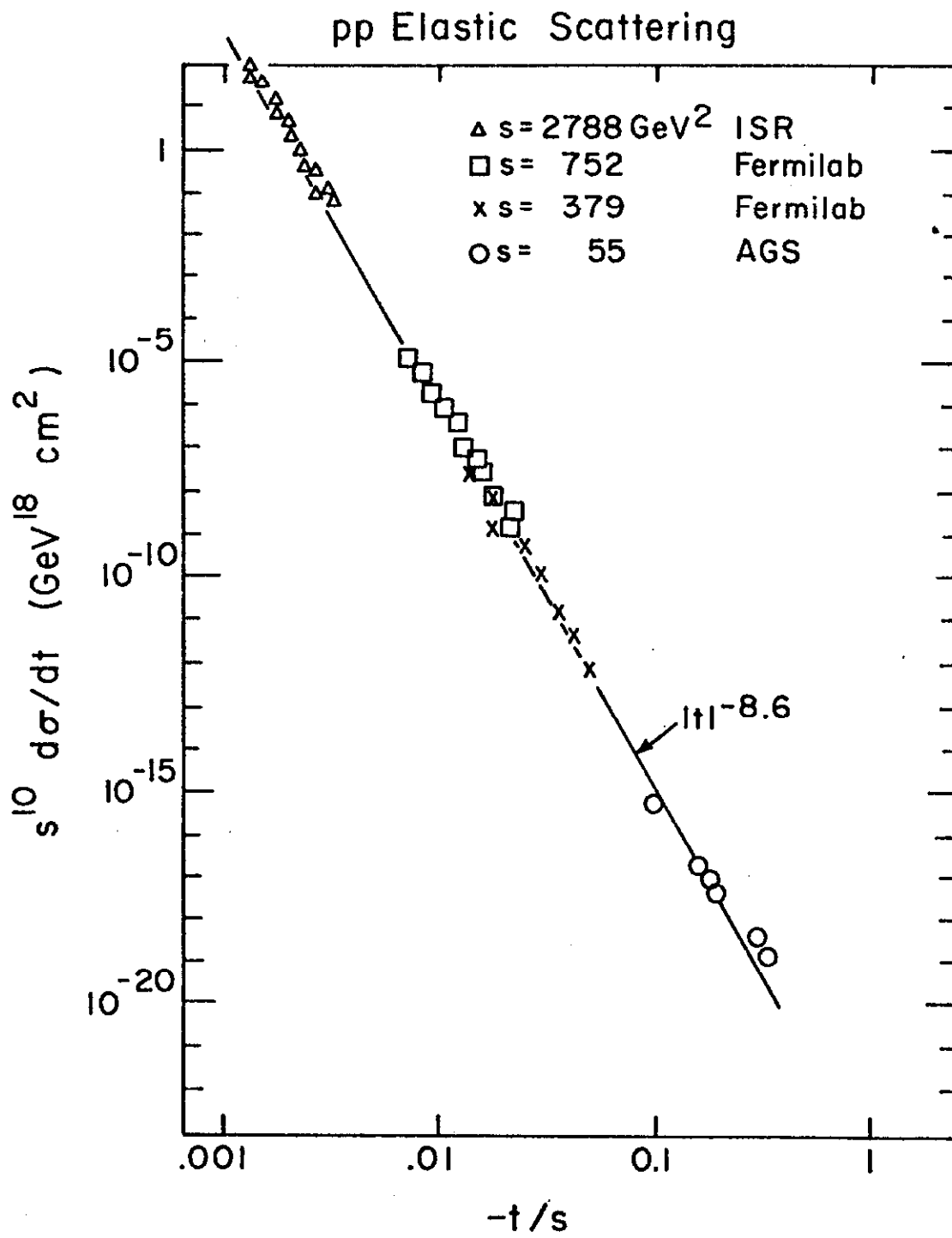


Figure 3

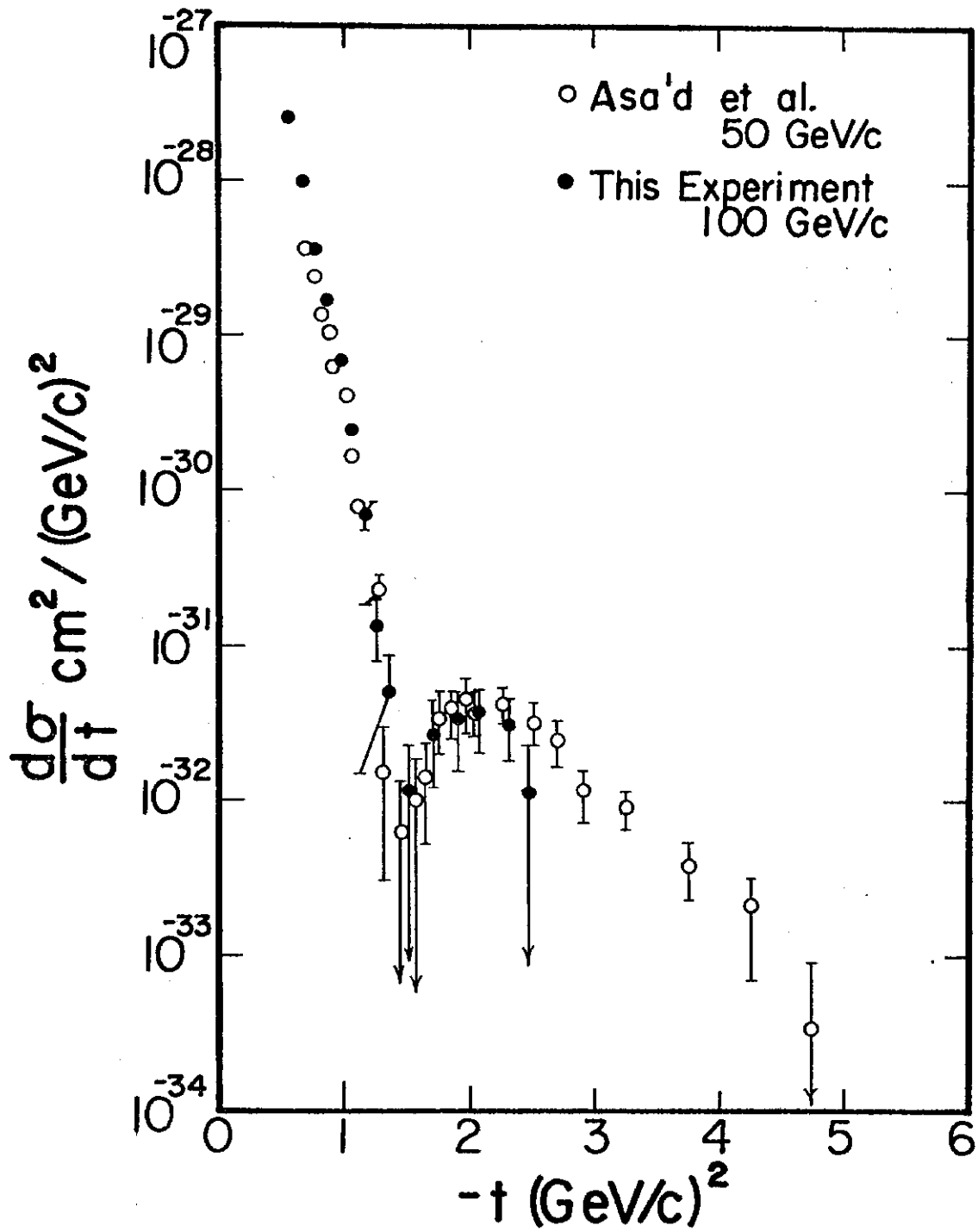


Figure 4

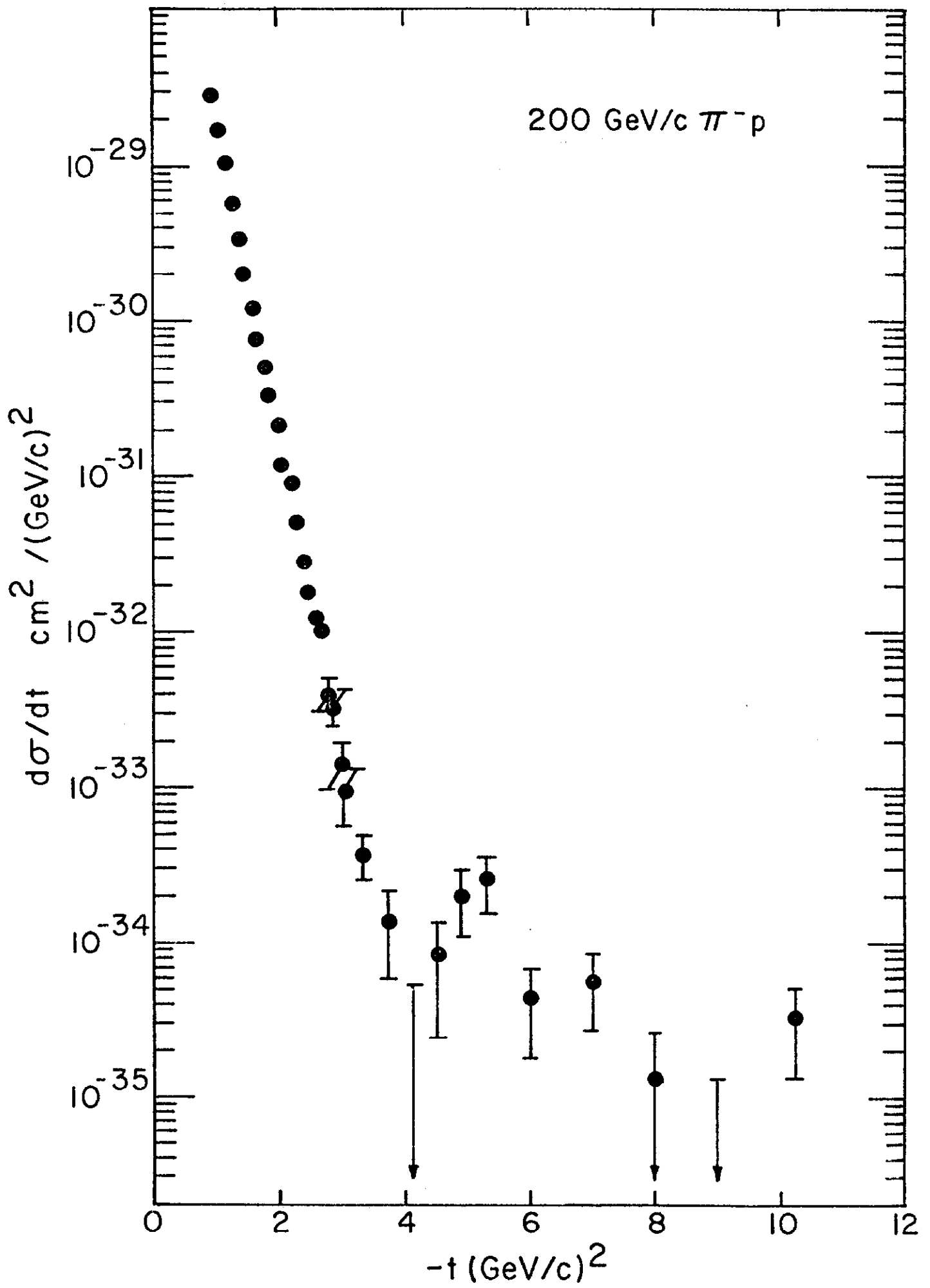


Figure 5

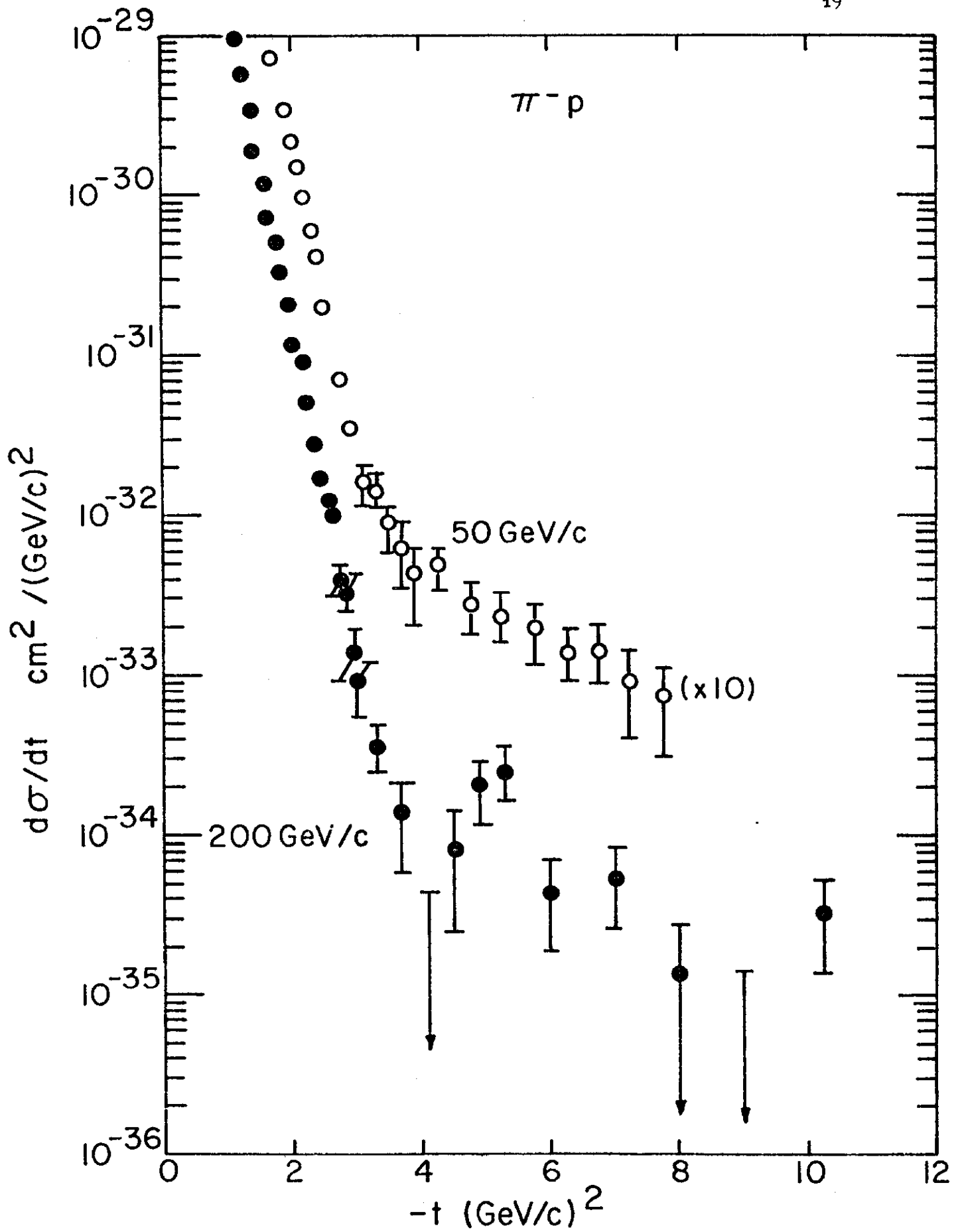


Figure 6

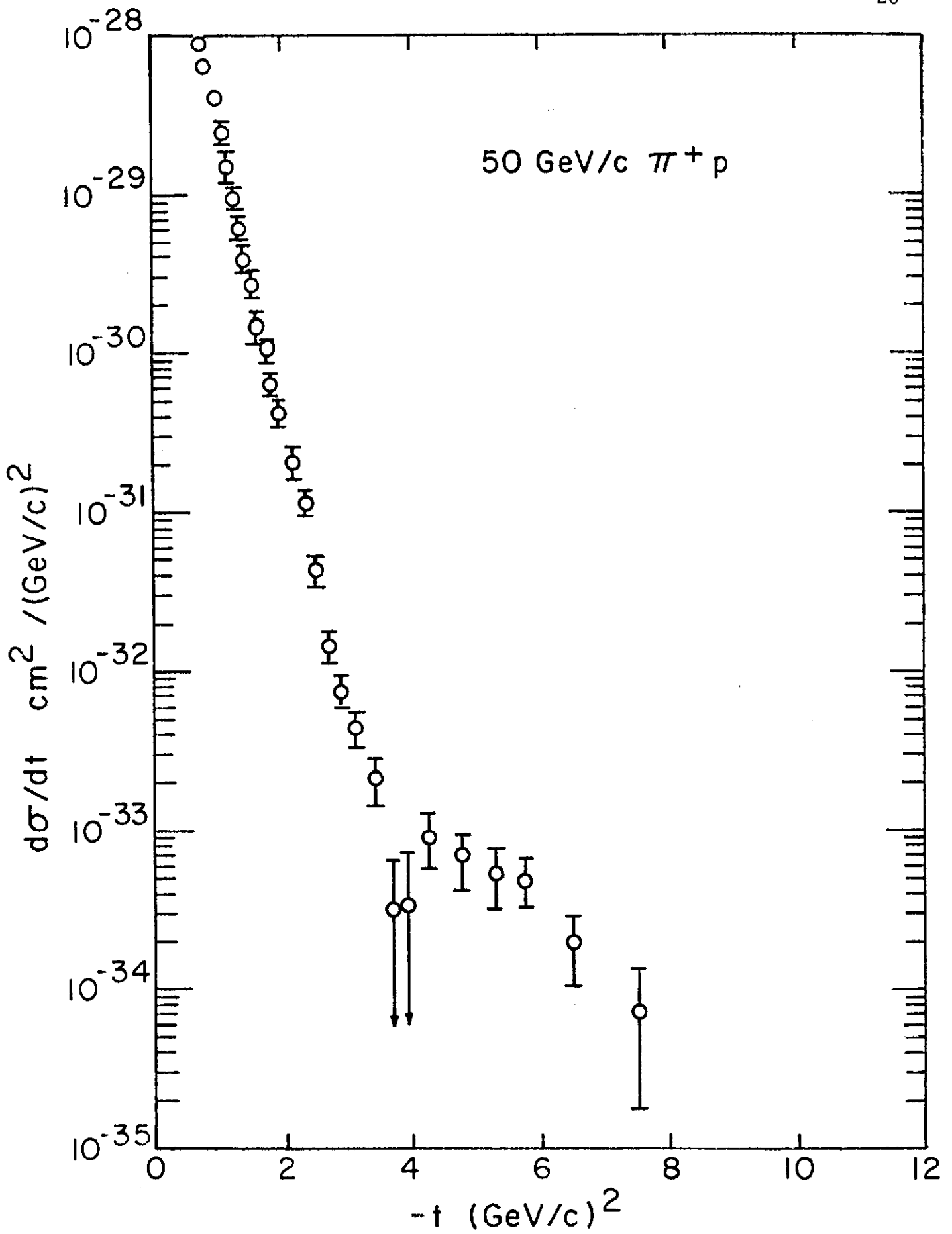


Figure 7

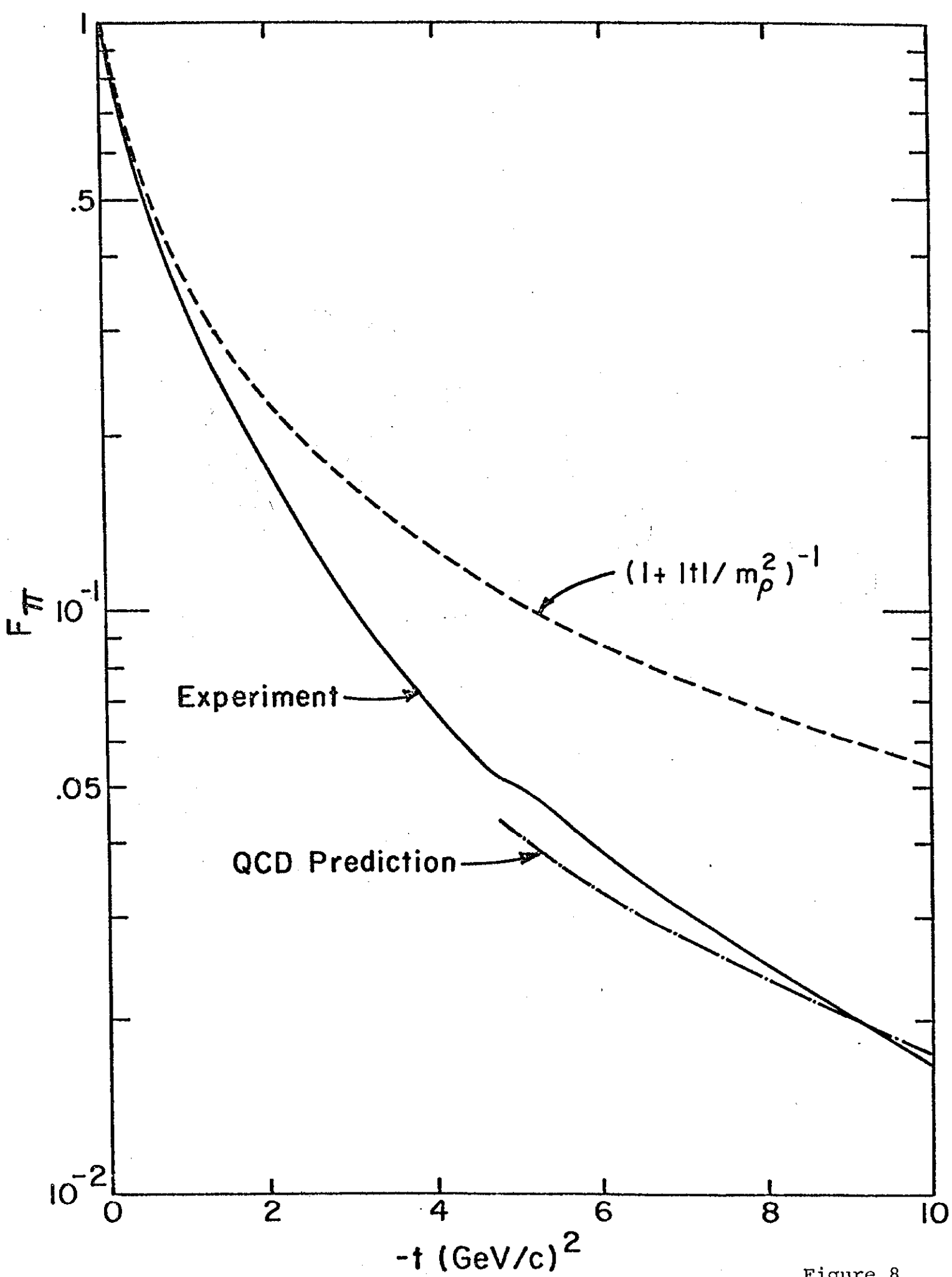


Figure 8

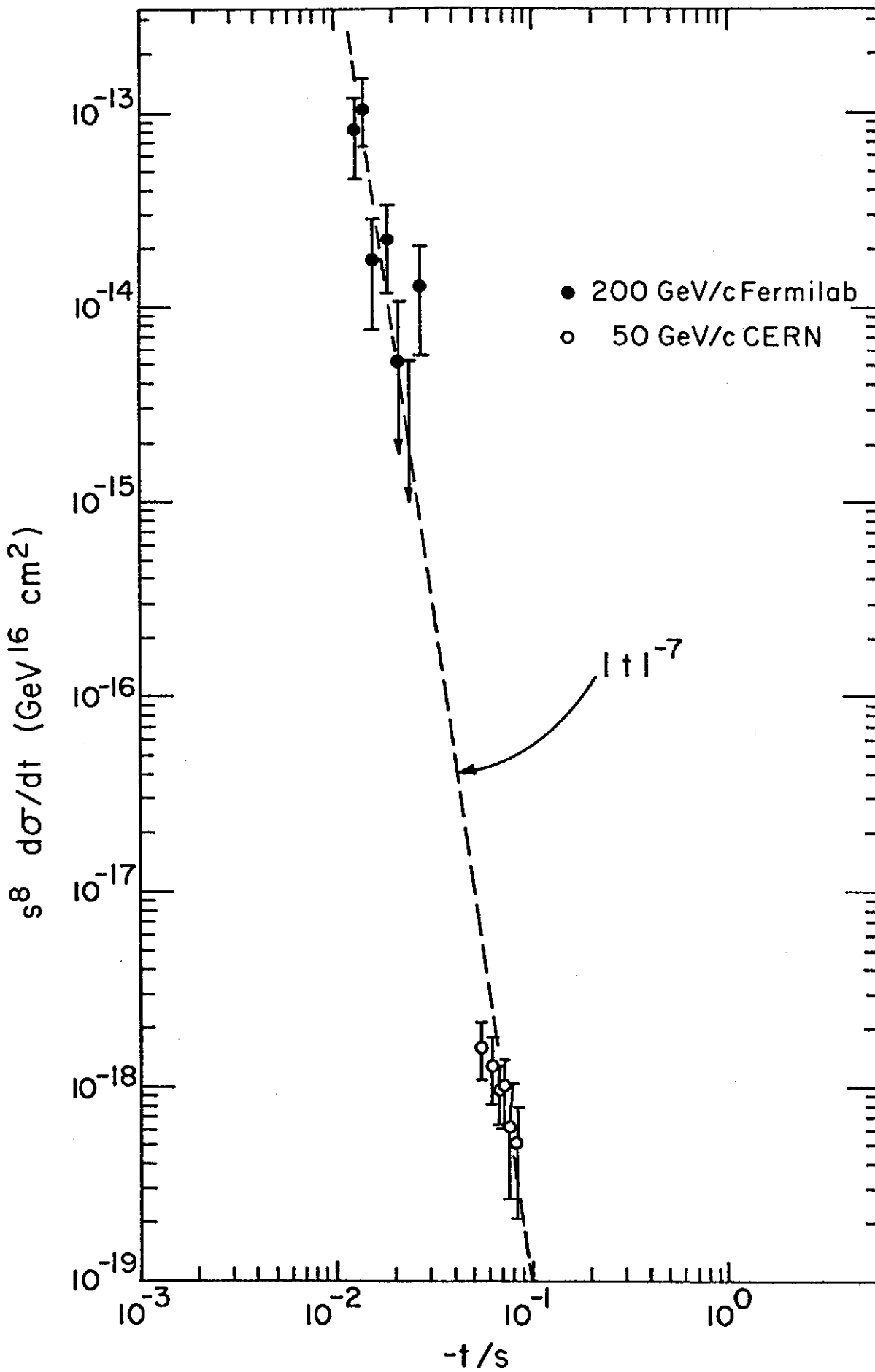


Figure 9

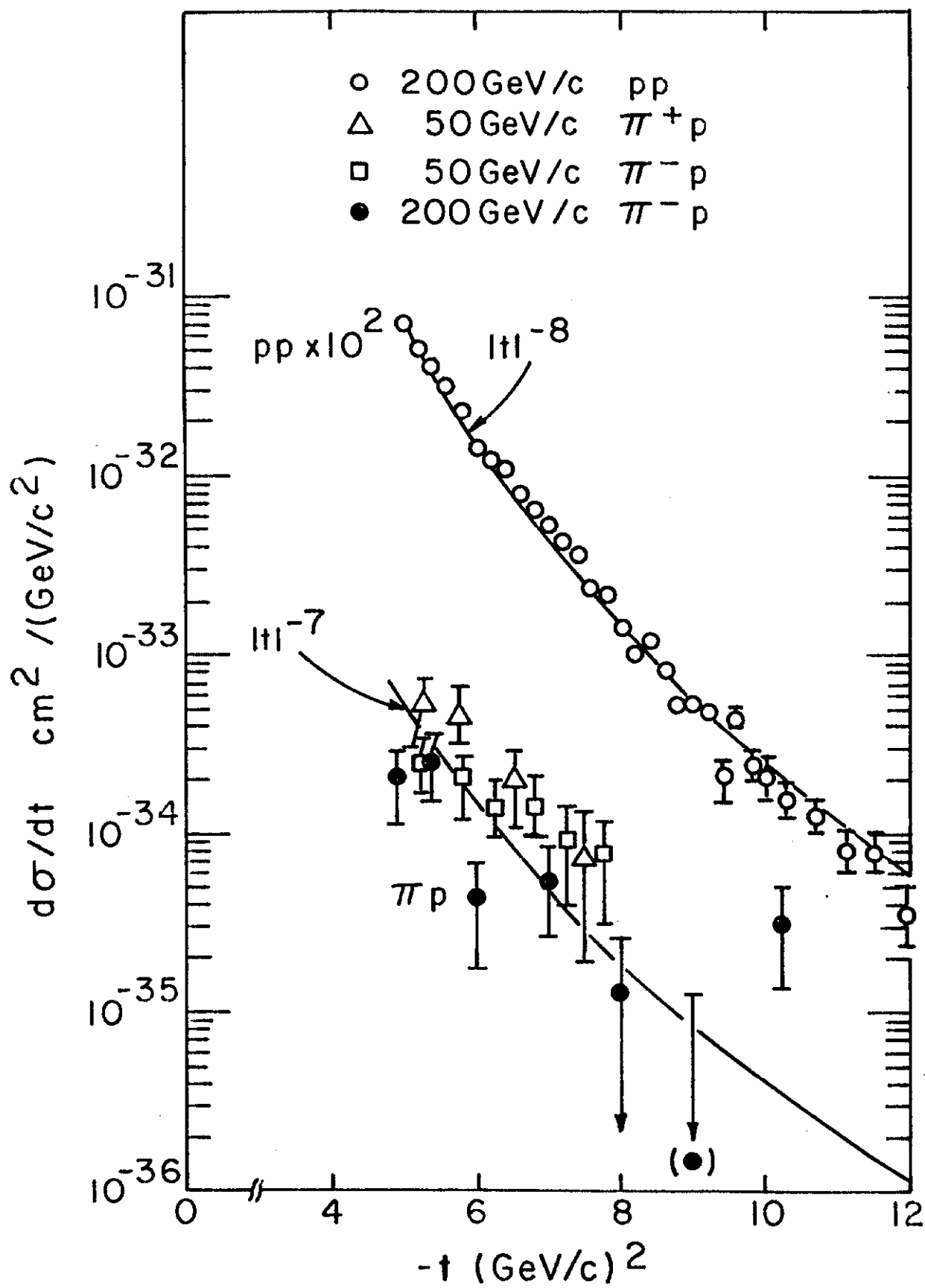


Figure 10

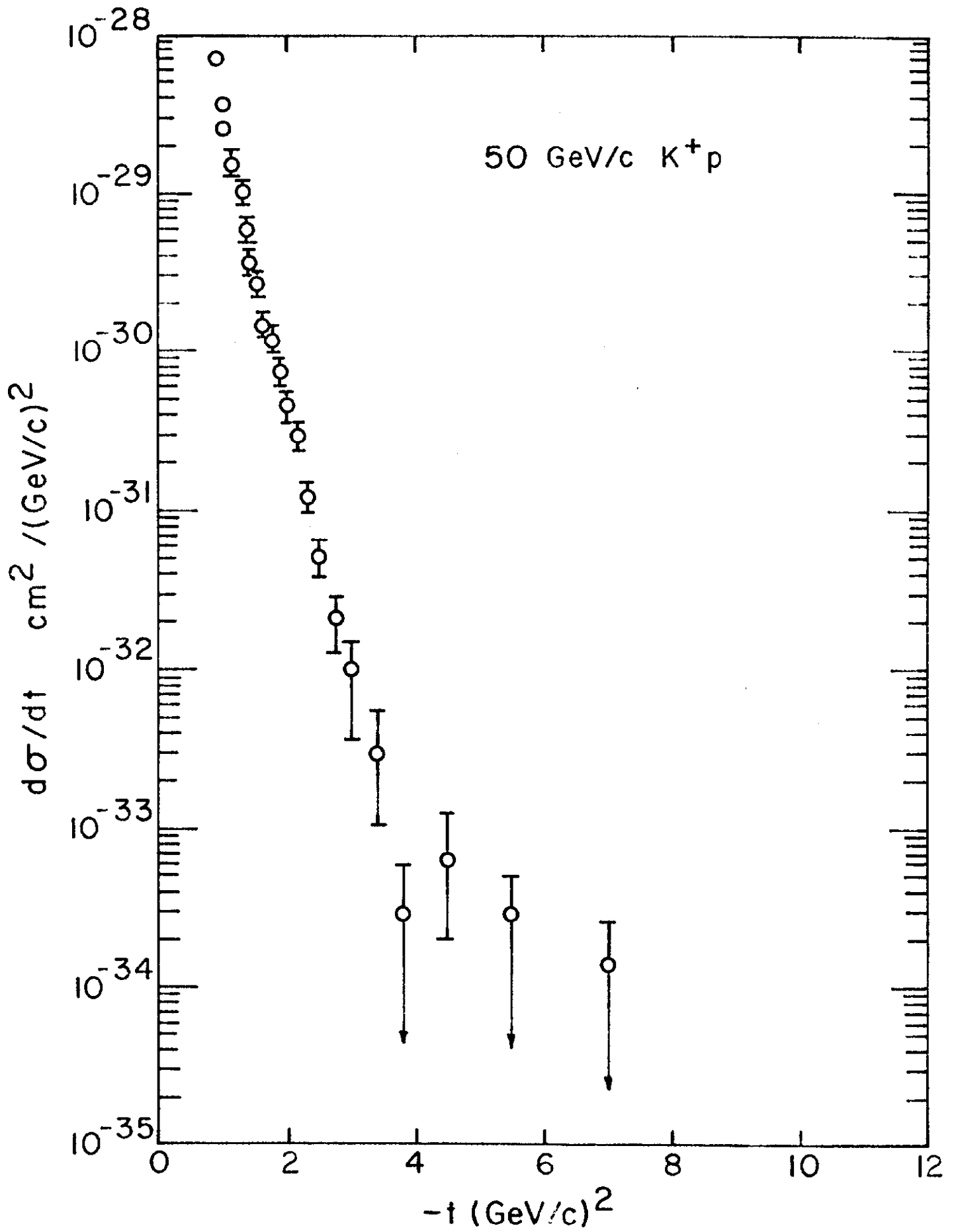


Figure 11

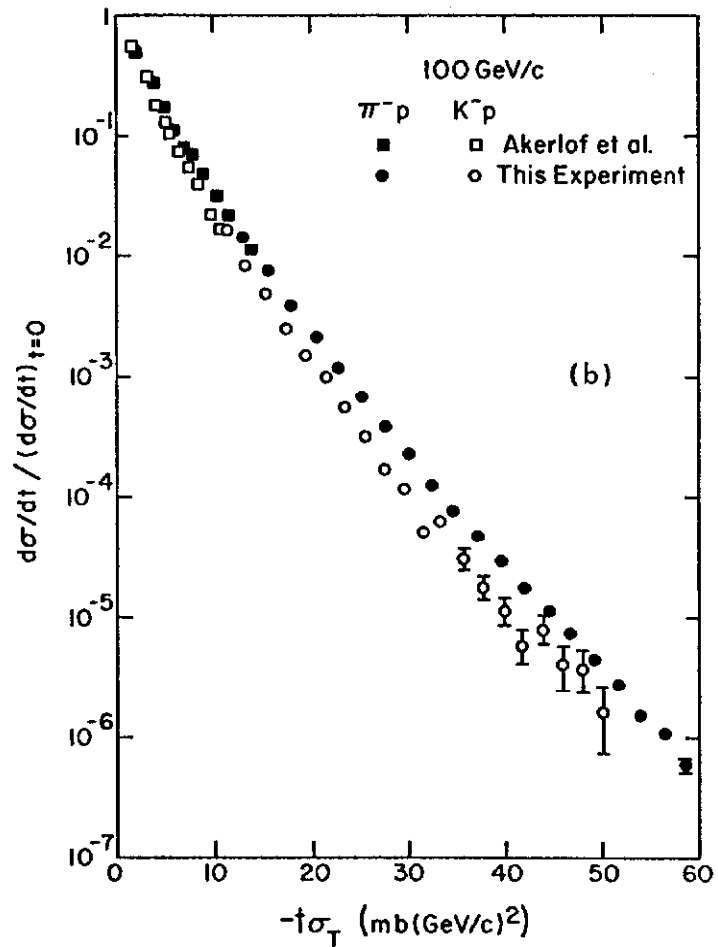
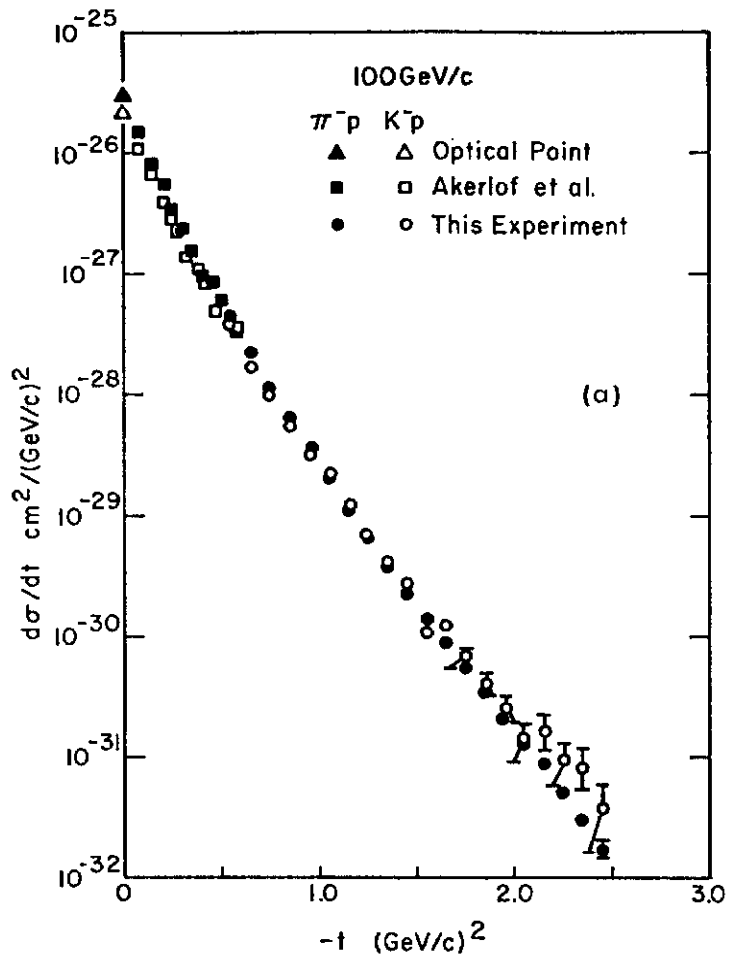


Figure 12

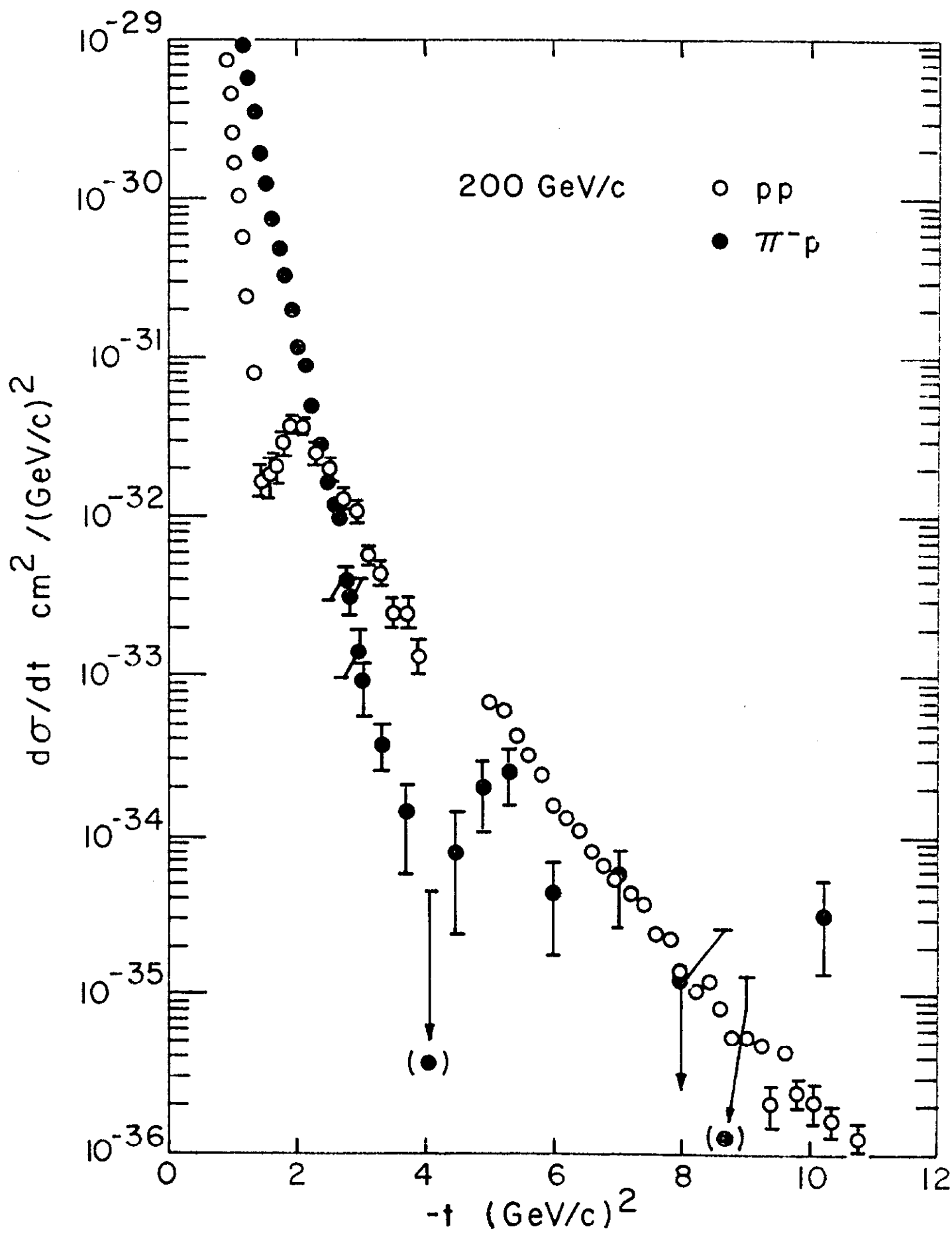


Figure 13